

# On the use of a heterogeneous MIMD-SIMD platform to simulate the dynamics of globular clusters with a central massive object

R. Capuzzo Dolcetta<sup>1</sup>, N. Pucello<sup>2,3</sup>, V. Rosato<sup>2,4</sup>, F. Saraceni<sup>2</sup>

<sup>1</sup>*Phys. Dept., Università di Roma "La Sapienza", P.le A. Moro 2, 00185 Roma (Italy)*

<sup>2</sup>*ENEA, Casaccia Research Center, HPCN Project, P.O. Box 2400, 00100 Roma (Italy)*

<sup>3</sup>*CASPUR, Università di Roma "La Sapienza", P.le A. Moro 2, 00185 Roma (Italy)*

<sup>4</sup>*Istituto Nazionale di Fisica della Materia (INFN), UdR Roma I*

---

The dynamics of a large stellar (globular) cluster containing  $N=128,000$  stars has been simulated by a direct summation ( $O(N^2)$ ) method by using a heterogeneous platform. Preliminary simulations have been carried out on model systems with and without the presence, in their center of mass, of a black hole whose mass has been varied from 0.02 to 0.1 times the total mass of the cluster. These simulations followed the evolution of the globular cluster in order to describe its dynamics over an interval of time sufficiently large respect to the internal crossing time. Computations have demonstrated that the platform heterogeneity, allowing a very efficient use of the computational resources, can be considered a key feature for sustaining large computational loads. Our results show that the massive object in the center of the cluster alters the surrounding star distribution very quickly; the following evolution is much slower as it occurs via two-body collisional relaxation.

---

*Key Words:* self-gravitating  $N$ -body simulations; heterogeneous MIMD-SIMD platform

## 1. INTRODUCTION

Although the main trend of high performance computing seems to focus on the assembly of larger and larger Massively Parallel Platforms (MPP) (e.g. the US ASCI platforms [1]), the design, the realization and the deployment of specialized (or dedicated) hardware is at the center of a renewed interest, particularly in the field of scientific applications.

In the recent years, several scientific domains have received a substantial impulsion by the use of specialized (or dedicated) hardware: the Lattice Quantum Chromodynamics (LQCD) model, thanks to the platforms realized in the frame of the APE [2, 3] and the Columbia projects [4], has significantly increased its prediction power. Computational astrophysics has received significant benefits by the use of the dedicated platform GRAPE (GRAVitational Pipe) [5] which is able to sustain a computational power of the order of Ter-

aflop/sec. in the gravitational  $O(N^2)$  calculations. More recently, the use of more complex N-body codes requiring a substantial amount of  $O(N \log N)$  calculations has triggered the development of new dedicated hardware, built by exploiting new programmable devices (FPGA), used in combination with the GRAPE machine (AHA-GRAPE project [6]).

Other dedicated and specialized hardware devices have been also conceived to improve the sustained computational power of numerical modeling in the field of 3-dimensional Ising models [7], [8], in that of molecular orbital calculation in quantum chemistry [9] and in molecular dynamics simulation of complex systems (e.g. biological matter) [10]. This list, far from being exhaustive, puts together both dedicated (non-programmable) and specialized (programmable) devices. Whereas dedicated architectures cannot be deployed in application fields different from those for that they have been conceived, specialized hardware (like e.g. the APE platform) can be usefully deployed also in different application fields.

In order to take the most from these platforms, their power is often exploited in conjunction with a host platform (a simple workstation or a general purpose parallel platform). In this configuration, the specialized/dedicated platform can be regarded as a smart co-processor of the host to which specific parts of the computation can be allotted. The resulting hardware is, thus, the *heterogeneous* sum of general-purpose and specialized/dedicated machines; it allows to produce very efficient calculations as different (in terms of algorithmic structure) parts of the code can be allotted to the parts of the architecture most suited to map their specific computational complexity.

This work has addressed two different issues.

The first is concerned with the astrophysical problem of simulating, with a reliable model, the dynamics of a large stellar cluster whose central region hosts a massive object (like a black hole). The aim is to apply these numerical models, which are approximated just in what regards the numerical time integration scheme, to the evolution of the cluster mass distribution over an interval of time of the order of ten crossing times (the *crossing time*  $t_c = 2R / \langle v \rangle$ , is the time required by the typical object of the system to cross the system, i.e. to cover a length scale equal to twice the initial radius of the system  $R$ , with a velocity  $\langle v \rangle$  equal to the average star's velocity). Actually, we estimate this interval of time as sufficient to sum up collective effects even if it is still short respect to the two-body relaxation time that is the 'graininess'-dependent time scale.

The representation of a large self-gravitating system with a particle model is, indeed, limited by the number  $N$  of particles that can be numerically handled; astrophysical self-gravitating systems span a range of  $N$  from 2 to  $10^{12}$  (see Table 1). The direct evaluation (i.e. that obtained by the sum of the contribution to the force on an object of the system by all the others without approximations with the exception of a possible smoothing of the interaction potential) of the N-body forces implies a restrictive limit to the number of bodies which can be treated (being the algorithm of a  $O(N^2)$  scaling). At present, the largest value of  $N$  that can be approached with such methods, on large computational platforms, is  $N \simeq 10^5$ . This means that a one-to-one representation of stars with simulating particles is now possible only for stellar systems up to a typical (not too populous) globular cluster (see Table 1). Larger systems can be treated with approximate methods such as *tree codes* [11], *particle-mesh*(PM) and *particle-particle, particle-mesh*(P<sup>3</sup>M) [12] algorithms.

The second aim of this work is to focus on the key role which could be played by heterogeneous platforms to efficiently cope with complex computational problems. In this case, an heterogeneous platform, made up by connecting a specialized architecture to a

TABLE 1

The table provides, for several astrophysical systems, the corresponding range of the number of stars in the system, the numerical approximation commonly used by simulations and the two-body relaxation time of the object in units of crossing time. The value of the relaxation time  $t_{rel}$  has been expressed in terms of the crossing time  $t_c$  by means of the relation  $t_{rel} \approx 0.1 \frac{N}{\ln N} t_c$ .

Stellar system	N	Numerical approximation	$t_{rel}/t_c$
OB associations	10-100	direct	1 – 5
Open clusters	100-1000	direct	5 – 30
Globular clusters	$10^5$ - $10^6$	direct	$10^3$ – $10^4$
Dwarf galaxies	$10^8$	tree-algorithm,PM,P3M	$10^7$
Galaxies	$10^{10}$ - $10^{12}$	tree-algorithm,PM,P3M	$10^8$ – $10^9$

general-purpose platform, is used in a computationally intensive computational problem. The efficient use of the platform (induced by a suitable mapping of the algorithm onto the machine architecture and the use of a smart communication scheme) has allowed to reach a sustained computational power of the order of 10 Gflop/sec, necessary to perform extensive calculations.

The scheme of the paper is the following. The next section provides a brief outlook of the heterogeneous platform used to perform computations. The definition of the physical model considered for the computations is the object of the third section, which also contains a schematic layout of the techniques used to implement the calculations on the computing architecture. The fourth and the fifth sections are devoted to the presentation and the discussion of the results. In these sections both the scientific relevance of the resulting data and the fate of the heterogeneous computing in complex scientific calculations are discussed.

## 2. LAYOUT OF THE COMPUTATIONAL PLATFORM

The heterogeneous platform used for computations is a MIMD-SIMD [13] platform, called PQE1 (Fig.1), realized in the frame of an industrial program by ENEA and QSW (an italian company of the Finmeccanica group) [14]. The PQE1 is a platform where the flexibility and the operability of a MIMD platform with a distributed-memory architecture are coupled to the power and the efficiency of SIMD machines. We assume that most algorithms arising in scientific applications are mainly expressible through synchronous programs with synchronous communications. These execute the same instruction on a set of different data which can be easily mapped onto a data parallel structure with regular patterns of memory access. Under these assumptions, it is reasonable to allot those parts to the SIMD machine, leaving the remaining tasks of the computation to be executed on the MIMD part. The PQE1 platform consists of a MIMD general-purpose platform, acting as a docking unit and of 7 SIMD machines.

The MIMD system is a Meiko/QSW CS-2 platform with 8 nodes, each of them based on a dual-HyperSparc processor at 125 MHz, connected in the SMP configuration by a Meiko/QSW proprietary network based on the Elan/Elite devices and implementing a multistage interconnection network with Fat Tree topology and point-to-point bandwidth

of 100 Mbyte/sec. This platform offers a peak speed of 2.18 Gflops/sec. and has about 2 Gbytes of addressable RAM.

The SIMD platforms come from the APE project (APE100 [2, 3]) and have been produced by QSW with the commercial name of Quadrics. The installed platforms have the following characteristics: two of them (called QH4) have 512 Floating Point Units (FPU) arranged as an (8x8x8) 3D torus and 5 of them (called QH1) have 128 FPU's, arranged as an (8x4x4) 3D torus. Each FPU is based on a custom VLIW processor, has clock frequency  $\nu=25$  MHz and is able to terminate a 'normal operation'  $A*B+C$  (where A, B and C are IEEE 754 standard, single precision, real numbers) every clock cycle. Each processor thus executes two floating point operations in one clock cycle (when the pipeline is full) and has a peak speed of 50 Mflops/sec. Each FPU is connected to a data memory of 4Mbytes and has an internal register file (RF) with 128 registers. Each clock cycle the processor is able to read two operands from RF and write one result to RF. Communications with other adjacent FPU's, connected in the north, south, east, west, up and down directions are synchronous and memory mapped. The interprocessor communication bandwidth is 12.5 Mbyte/sec, so the 512 (128) processor configuration has an aggregate bandwidth of 6.4 (1.6) Gbyte/sec and a peak speed of 25.6 (6.4) Gflops/sec.

The SIMD APE100/Quadrics machines are connected to the MIMD system through an HiPPI (High Performance Parallel Interface) channel, which provides a bandwidth of 20 Mbyte/sec. Each MIMD node is connected to a different SIMD platform, as in the scheme of the complete prototype reported in Fig.1. Looking at previous data, it is clear that the machine is strongly unbalanced, having the most of computational and communication speed in the SIMD part.

The rationale for the design of such a prototype platform is related to the necessity of having a complex computing platform whose complexity mirrors that of the computational codes used in scientific applications. These latter are, in fact, formed by a sequence of tasks, each of them characterized by a *task granularity*  $g_t$  given by

$$g_t = \frac{N_{op}}{D_{I/O}} \quad (1)$$

where  $N_{op}$  is the number of floating point operations to be performed and  $D_{I/O}$  is the I/O data to be processed in the task. Analogously, it is possible to define a *machine granularity*  $g_m$  given by

$$g_m = \frac{F_{op}}{B} \quad (2)$$

where  $F_{op}$  is the computational power of the platform and B its I/O bandwidth. It has been proven [15] that an efficient implementation of the task on a given computational platform implies that

$$g_m < \eta g_t \quad (3)$$

where  $\eta$  is a suitable factor  $0 < \eta < 1$  expressing the efficiency of the task implementation. For this reason, an efficient implementation of a complex computational code

implies the simultaneous presence of a complex computational structure able to satisfy the requirement of eq.(3) for each task composing the code. The complexity of the PQE1 platform is thus exploited by allotting the high-granularity tasks to the SIMD part and the low-granularity and the pre/post processing tasks to the MIMD machine.

### 3. MODEL AND COMPUTATIONS

We represent the stellar system as a set of  $N=128,000$  point-masses (stars) interacting via the classical pair gravitational potential

$$V(r_{ij}) = -G \frac{m_i m_j}{r_{ij}} \quad (4)$$

where  $r_{ij}$  is the distance among the  $i$ -th and  $j$ -th star of the system. The stellar masses are assumed all equal. To avoid force divergence, the interaction potential  $V$  has been smoothed by substituting  $r_{ij}$  with  $r'_{ij} = r_{ij} + \epsilon$ . The introduction of the smoothing parameter  $\epsilon$  affects the dynamics on that length scales. This distance, in general, is set to smaller values than the average interparticle distance, in order to ensure an acceptable level of approximation of the system's dynamics.

When a massive object is present in the system (as a massive black hole) another length scale is naturally introduced in the problem: the tidal radius  $r_t = (\frac{m_{BH}}{2m})^{\frac{1}{3}} R_*$ . A star of mass  $m$  and radius  $R_*$  approaching a black hole (of mass  $m_{BH}$ ) at a distance smaller than  $r_t$  is destroyed by the strong tidal deformation and, consequently, its mass goes to increase that of the black hole with a positive feedback on the tidal radius. Our computational code takes into account the possibility that a star is swallowed by the massive object which accordingly increases its mass and its  $r_t$ . However,  $r_t$  is usually much smaller than the typical interstellar distance so that  $m_{BH}$  remains almost unchanged throughout the simulations.

The initial spatial distribution of the  $N$ -stars of equal masses has been sampled by a spherical Plummer distribution (see [17])

$$\rho(r) = \frac{\rho_0}{[1 + (\frac{r}{r_c})^2]^{\frac{5}{2}}} \quad (5)$$

where the central density  $\rho_0$  and the "core" radius  $r_c$  are free parameters. The initial stars velocities have been obtained self-consistently, from the velocity distribution function that generates the Plummer's density law, i.e.

$$f(\mathbf{r}, \mathbf{v}) = \begin{cases} (-E)^{7/2}, & E \leq 0 \\ 0, & E > 0 \end{cases} \quad (6)$$

where  $E = 1/2v^2 - \phi(r)$  is the individual star's energy in the (spherical) potential  $\phi(r)$  given by the Plummer mass distribution. The star velocities distributed according to eq. (6) are scaled to have a virial ratio  $Q = 2T/|\Omega| = 0.98$  (where  $T$  and  $\Omega$  are the kinetic and the gravitational energies of the system) where the equilibrium value is 1; the inclusion of a black hole with mass 0.02 and 0.1 of the total star mass at the center of mass changes the virial ratio to  $Q = 0.87$  and  $Q = 0.75$ , respectively, inducing a stronger gravitational collapse.

The equations of motion have been integrated by using the central difference Verlet–scheme [16] with a fixed time–step . This scheme allows an accuracy of order  $\Delta t^4$  in the positions and  $\Delta t^2$  for the velocities. The time step  $\Delta t$  has been empirically selected by requiring the relative error of the total energy to be smaller than  $10^{-4}$  per time step. It results that  $\Delta t$  is a fraction of the system’s crossing time,  $t_c$ . After having fixed the value of  $\epsilon$ , several simulations have been carried out, with different values of  $\Delta t$ , up to the value which allowed to obtain the relative error of the total energy in the desired range.

The part of the PQE1 platform selected for the calculations consists of a single MIMD node and a QH4 platform. The MIMD node has been used to perform data initialization, the evaluation of the component of the star forces arising from the interaction with the black hole, the solution of the equations of motion and the evaluation of the relevant physical quantities (total and potential energy, virial ratio, Lagrangian radii, mass and velocity distributions). The  $O(N^2)$  force-loop has been, in turn, implemented on the QH4 platform. For this purpose, a number of stars  $N_p=N/n_p$  (where  $n_p=512$  is the number of FPU of the QH4 platform) has been allotted to each FPU. The force calculation has been performed by making use of a recently developed hyper-systolic algorithm [18] in order to exchange data among the processors. This scheme allows reduction of the redundancy typical of the systolic algorithm [19], thus allowing to save a substantial amount of computing time.

In the systolic-type algorithms, there is a regular sequence of calculation and communication steps. In our case, after the allocation of equal groups of  $N_p$  stars on each FPU, the code evaluates the  $N$ –body forces within each group. A copy of the positions of each group is then moved, from the initial to the next neighbor FPU and, there, interacted with the resident group of stars. The process is repeated until each group of stars has visited each other FPU. On each FPU is thus cumulated the force acting on the resident group of stars.

The  $O(N^2)$  problem requires, given  $N$  data elements being distributed among  $p$  processors, a number  $O(Np)$  of inter-processor communications, i.e.  $O(N)$  communications per processor. As this often leads to severe performance bottlenecks, it is mandatory to search for new algorithms that are able to reduce inter-processor communications to a number  $O(N)$  per processor.

The hyper-systolic algorithm, recently introduced, has the potential to decrease inter-processor communications for computational problems of the type mentioned above to a number  $O(N^{\frac{1}{2}})$  per processor. This is achieved by a 1-dimensional systolic mapping of the data onto the processing elements and the use of shortcut inter-processor communication (hyper-connections) together with a replicated systolic mapping of data.

The basic feature of hyper-systolic computing is a sequence of shifts called HS-base which represent the hyper-systolic strides along the 1-dimensional chain to be performed in the hyper-systolic parallel calculation. The direct computation of *optimal* bases is exponentially expensive, with the number of processors  $p < 64$ . For larger numbers of processors, hitherto, aside to the so-called *regular* bases, new HS-bases have been determined [20] with a search technique based on Simulated Annealing.

The implementation of the hyper-systolic communication scheme on the  $N^2$  calculation on the 512-node Quadrics QH4, has allowed to achieve about 20 % improvement in inter-processor communication compared to the regular base implementation.

The chosen implementation strategy allows to exploit a double level of parallelism: the first, consisting of the parallel implementation of the interstellar force calculation in the SIMD platform by the hyper-systolic algorithm, the second one related to the concurrent

black hole-stars force calculation performed by the host part during the time spent by the SIMD machine to produce the interstellar force.

The machine performance was such to allow an execution time  $t_{ex}=120$  sec. for the calculation of the single time-step of the cluster dynamics, by using the mentioned PQE1 partition. About 20% of this time is related to different communication actions (to/from the SIMD machine and within the SIMD machine, in the hyper-systolic loop), the residual time being spent for the number-crunching activity. The efficiency of the SIMD code (in terms of efficiency of use of the single FPU resources) was around 30%, thus leading to a sustained computational power, in the SIMD part, of about 9 GFlops/sec.

#### 4. COMPUTATIONAL DETAILS AND RESULTS

Three model systems have been simulated, all of them containing  $N=128000$  masses. The first one represents the globular cluster without any massive object; this system has been retained as reference and its behavior compared to that of the other systems. The second system contains a black hole of mass  $m_{BH}=0.02$  (in units of the total star mass) located at the center of mass of the cluster. The third system contains a black hole with  $m_{BH}=0.1$ . We express the model parameters taking as units of length and mass the initial radius of the system and its total mass, respectively. Moreover, setting  $G=1$  implies that  $t_c$  is the time unit. In these units, the value of  $\epsilon = R/500 = 0.002$  that we choose is much smaller than the average inter-particle distance (which is  $\propto n^{-1/3}$ , with  $n$  average number density); this guarantees an acceptable spatial resolution and keeps the newtonian behavior of the interparticle force. In the case of the unperturbed cluster (without the black-hole) a  $\Delta t=t_c/250$  has been used. The constraint imposed to the numerical scheme to ensure an energy conservation of at least  $10^{-4}$  per time step implied the use of a smaller time step ( $\Delta t=t_c/500$ ) when a black hole is present. In all cases, the systems have been simulated during a time interval of 10 crossing times.

The first reported quantity is the virial ratio  $2T/|\Omega|$  of the system (Figs. 2, 3 and 4). This quantity provides a first picture of the global dynamics in the cluster driven by the initial unbalance between kinetic and potential energy. The virial ratio is strongly perturbed by the presence of the massive object. This produces a strong driving force which brings the mass distribution to a virial equilibrium that is slightly different from  $2T/|\Omega| = 1$  due to the non-homogeneity of the interaction potential function induced by the presence of the softening parameter  $\epsilon$ . For the most massive black hole here considered ( $m_{BH} = 0.1$ ) the virialization is achieved more rapidly.

The virialization process is due to a violent relaxation that occurs as a consequence of a series of damped (non-adiabatic) oscillations of the system (see Fig. 5).

The evolution of both the spatial and projected density radial distributions are shown in Figs. 6 to 9 where the initial and final ( $t = 10t_c$ ) profiles are reported. The time evolution leads to a steepening of the profile toward the cluster center ( $r < 0.1$ ) more pronounced at larger black hole mass and to the population of a ‘halo’ ( $r > 1$ ) of high velocity stars. Both the external profile and the inner one (the latter evolving, of course, just in presence of the central compact object) are attained in a short time, of the order of one crossing time.

The slope of the space density inner distribution is for  $m_{BH} = 0.1$  at  $t = 10t_c$ ,  $-0.92$ , i.e. intermediate between the values  $-3/2$  and  $-1/2$  characteristic, respectively, of the density cusps analytically (and approximately) evaluated for the distribution of stars bound to a black hole and of those unbound [21]. We note that the slope of the halo region closely matches the expected  $r^{-2}$  profile (see, for instance, [22]).

The dynamical evolution of the model clusters is also characterized by the appearance of some anisotropy in the velocity distribution in the external regions. This has been characterized by the evaluation of the anisotropy parameters

$$\beta_\theta = 1 - \frac{\langle v_\theta^2 \rangle}{\langle v_r^2 \rangle}$$

$$\beta_\phi = 1 - \frac{\langle v_\phi^2 \rangle}{\langle v_r^2 \rangle}$$

(the  $\langle . \rangle$  averages represent the dispersions of the polar components of the velocity) as functions of the radial distance (see Figs. 10, 11 and 12). Being the initial distribution function given by Eq. (6) only dependent on the energy, the initial velocity distribution is obviously isotropic, and both  $\beta_\theta$  and  $\beta_\phi$  are zero (the three polar components of the velocity being the same, in the average). The behaviour of  $\beta_\theta$  and  $\beta_\phi$  is very similar for we expect the evolution keeps the velocity vector invariant for rotation around the plane orthogonal to the radial direction. We have thus plotted in Figs. 10 to 12 just  $\beta_\theta$ . It is evident, in all the cases studied, a rapid increase of  $\beta$  in the outer regions, where, indeed, orbits are more radially pointed due to the expansion of the stellar halo. Moreover, we note that the more massive is the central object the more evident is the negative minimum of the anisotropy parameter around the initial boundary. In the case  $m_{BH} = 0.1$ , the transverse components of the velocity dominate over the radial ones so to have  $\beta \simeq -1$ ; this means that a quick effect of the instability caused by the massive object is that the transverse "temperature" doubles the radial. This seems a transient effect because, as the evolution goes on, the radial dependence of the  $\beta$  parameter tends to be rather insensitive to the mass of the central object. At  $t = 10t_c$ , the isotropy is partially restored in the average, being still evident a radially biased distribution of orbits in the outskirts.

Finally, Fig.13 is a snapshot, at  $t = 10t_c$ , of the star distribution projected onto a coordinate plane of the model cluster having the  $m_{BH} = 0.1$  black hole at its center.

## 5. DISCUSSION AND CONCLUSIONS

Concerning with the main questions which have stimulated this work, it is possible to draw the following conclusions:

- the *heterogeneity* of the PQE1 platform can provide significant benefits also in the gravitational N-body calculations, although the structure of the computational problem is very different from that for which the SIMD platform Quadrics/APE100 has been conceived. This result confirms the relevance of the relation of eq.(3) which should be considered as the most important constraint to be fulfilled in the mapping of a code onto a computational platform.

The reported data confirms, in fact, that the increase of computational efficiency provided by heterogeneous platforms (where different architectures can coexist and provide an ideal computational frame to execute different parts of the complex computing codes characterized by different algorithmic complexity) can be seen as a key feature for high performance computing whose benefits should be more attentively searched and exploited.

The achieved sustained computational power allows to perform the simulation of the dynamics of one crossing time (with  $N=128,000$ ) in a wall clock time of the order of

$6 \cdot 10^4$  sec.; this figure allows to perform simulations of the order of tens of crossing times. The new SIMD machine, derived from the INFN project APEmille and constituting the follow-up of the Quadrics/APE100 platform, will enhance the computational power of a factor ten. This will permit to study the evolution of the cluster over a time of the order of hundreds of crossing times, i.e. of the order the two-body relaxation time.

- from the astrophysical point of view, this work has an introductory relevance to the ‘direct’ study of the dynamics of populous stellar systems (up to the scale of globular clusters) whose internal density varies over a range of scales such that approximations in the interaction potential (as multipolar expansions, solution of Poisson’s equation on a grid, etc.) are of questionable reliability. By the way, this work has shown how the inclusion of a massive object in a quasi-equilibrium model of a globular cluster, represented as a set of  $N=128,000$  stars interacting with the ‘exact’ potential (even if smoothed on a scale smaller than the average interstellar distance), has consequences on the overall dynamics. It induces a violent relaxation within few crossing times, corresponding to an evolution of the star radial distribution toward a central peaked distribution close to  $\rho \propto r^{-1}$  in the case of the most massive black hole considered  $m_{BH}=0.1$ . Another effect caused by the presence of the massive object is the loss of isotropy in the velocity distribution, both in the outer regions, where radial orbits dominate, and in an intermediate zone where, on the other side, transverse component of the velocity prevail. The inner region stands isotropic throughout the evolution.

We have stored the phase-space trajectories of the stars all along the simulated time. These data will allow a deeper investigation of the dynamical processes occurring at the early stages of the evolution and a careful characterization of the average properties of the stellar phase-space distribution.

### ACKNOWLEDGMENTS

The authors kindly acknowledge discussions and suggestions from R. Spurzem and M.Hemsemdorf (ARI, Heidelberg), P. Mocchi (Univ. of Roma) and P. Spinnato (DAS, Amsterdam). P. Palazzari and M. Coletta (ENEA, Roma) are gratefully acknowledged for their help in the implementation of the hyper-systolic algorithm. Part of this work has been supported by a INFN/PQE2000 grant to one of us (NP), performed under the frame of the PQE1 project (ENEA-QSW) and partially supported by CASPUR.

### REFERENCES

1. see <http://www.llnl.gov/asci>.
2. A.Bartoloni et al., Int. J. of Mod. Phys. C **4** (1993) 969.
3. A.Bartoloni et al., Int. J. Mod. Phys. C, **4** (1993) 955.
4. I. V. Arsenin, Nucl. Phys. B (Proc. Suppl.) **42**, 902 (1995).
5. J. Makino, M. Taiji, T. Ebisuzaki, D. Sugimoto, Astrophys. J. **480**, 432 (1997).
6. R. Spurzem, J. Comput. Appl. Math. **109**, 407 (1999).
7. R. H. Swendsen, J. S. Wang, Phys. Rev. Lett. **58**, 86 (1987);
8. A. L. Talapov, H. W. J. Blote, L. N. Shchur, JETP Lett. **62**, 174 (1995).
9. S. Shirakawa, T. Yoshii, K. Murakami, U. Nagashima, S. Obara, T. Amisaki, K. Kitamura, H. Takashima, K. Tanabe, Technical Report of IEICE, CPSY96-46, (1996) p.45-50.
10. see informations on the C4 cluster at the ETH Zurich at the web site <http://igc.ethz.ch/c4/C4-cluster.html>.
11. J. Barnes, P. Hut, Nature **324**, 446 (1986);
12. R.W. Hockney, J.W. Eastwood, *Computer simulation using particles*. Adam Hilger pub., Bristol, U.K. (1988)

13. The acronyms MIMD and SIMD refer to parallel platforms working in an asynchronous way (Multiple Instruction Multiple Data) and in a synchronous way (Single Instruction Multiple Data).
14. see the web page [http : //www.enea.it/hpcn/PQE1](http://www.enea.it/hpcn/PQE1).
15. P. Palazzari, L. Arcipiani, M. Celino, R. Guadagni, A. Marongiu, A. Mathis, P. Novelli, IEEE Proceedings of the 9th Heterogeneous Computing Workshop (May 1–5 2000, Cancun, Mexico),
16. L. Verlet, Phys. Rev. **159**, 98 (1967).
17. H.C. Plummer, Mon. Not. Roy. Astron. Soc. **71**, 460 (1911).
18. T. Lippert, U. Glasser, H. Hoerber, G. Ritzenhofer, K. Shilling, A. Seyfried, Int. J. Mod. Phys. C **7**, 485 (1996).
19. N. Petkov, *Systolic Parallel Processing*, North Holland, Amsterdam (1992)
20. T. Lippert, P. Palazzari, K. Schilling, NATO Advanced Workshop on High Performance Computing: Technology and Applications, Cetraro, Italy, June 24-26, 1996.
21. J. Binney and S. Tremaine, 1987. *Galactic Dynamics*, Princeton Series in Astrophysics, Princeton Univ. Press (Princeton, N.J.)
22. S. L. Shapiro, A. P. Lightman, Nature **262**, 743 (1976).

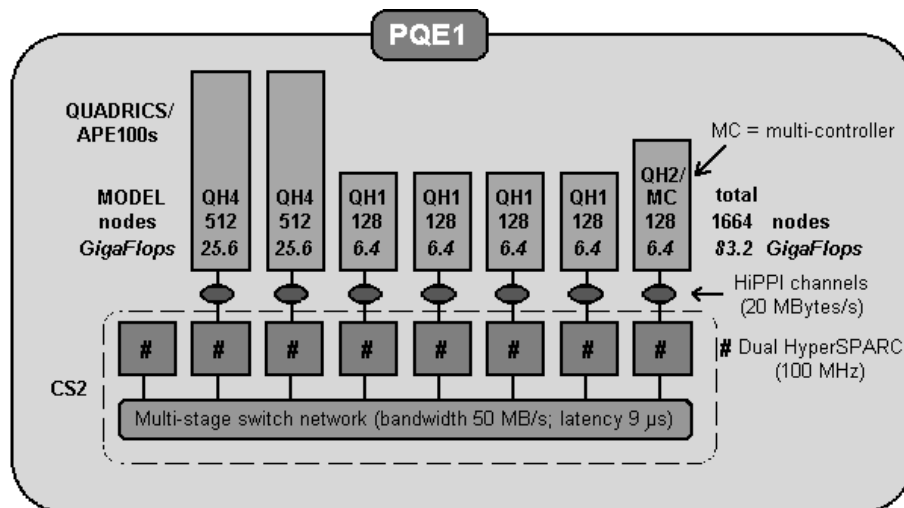


**FIG. 1.** Schematic layout of the PQE1 platform. The proprietary multi-stage switch network of the CS2 platform has a fat tree topology. Aside to the Hippi channel, there is a Transputer-based link which allows communications to occur between the CS2 node and the connected SIMD platform.

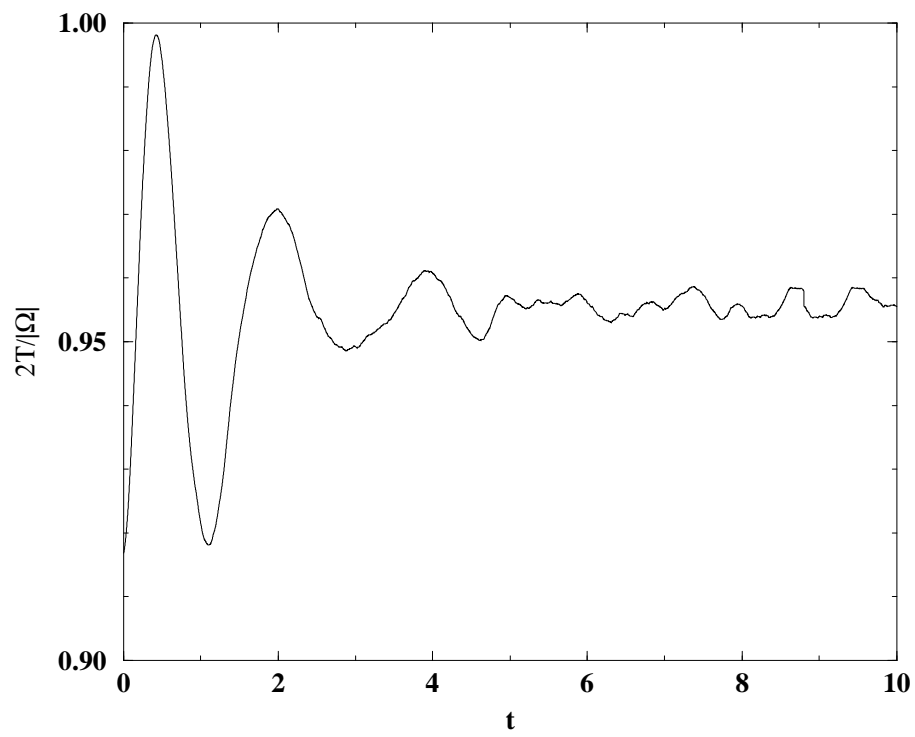


**FIG. 2.** Virial ratio,  $\frac{2T}{|\Omega|}$ , as a function of time, for the system without the black-hole. Time is expressed in units of crossing time  $t_c$ .

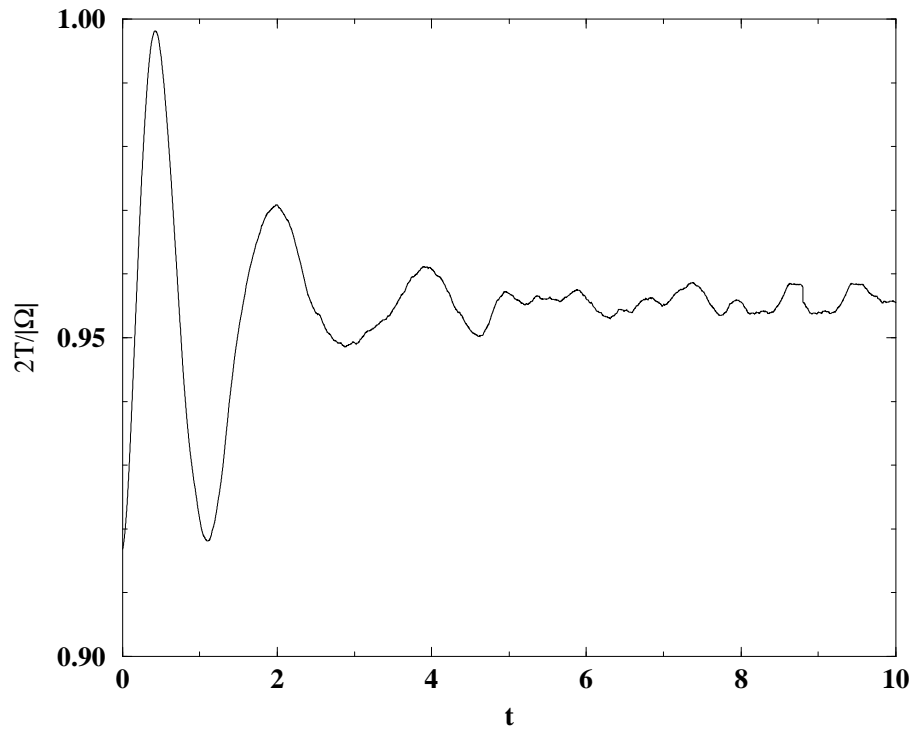


**FIG. 3.** Virial ratio,  $\frac{2T}{|\Omega|}$ , as a function of time, for the system with the black-hole of mass  $m_{BH}=0.02$ . Time is expressed in units of crossing time  $t_c$ .

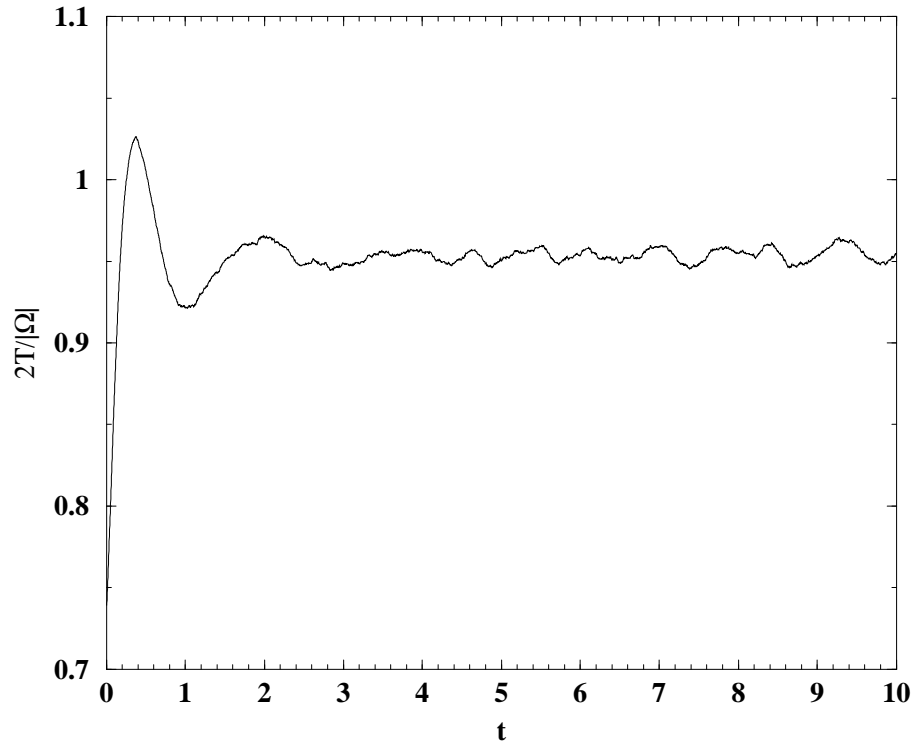


**FIG. 4.** Virial ratio,  $\frac{2T}{|\Omega|}$ , as a function of time, for the system with the black-hole of mass  $m_{BH}=0.1$ . Time is expressed in units of crossing time  $t_c$ .

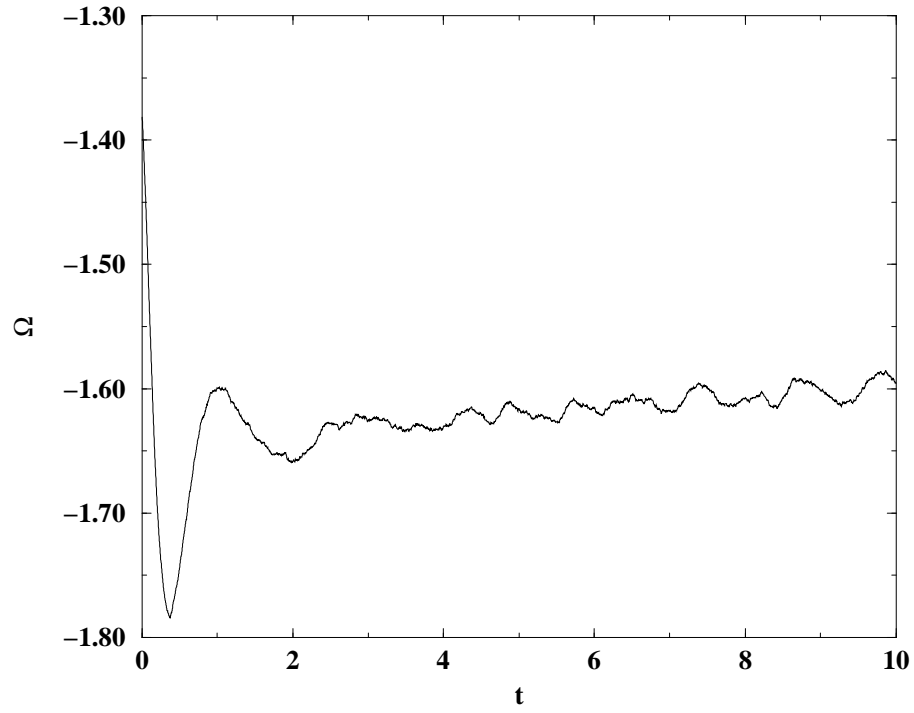


**FIG. 5.** Total potential energy  $\Omega$  vs. time for the system with the black-hole of mass  $m_{BH}=0.1$ . Time is expressed in units of crossing time  $t_c$ .

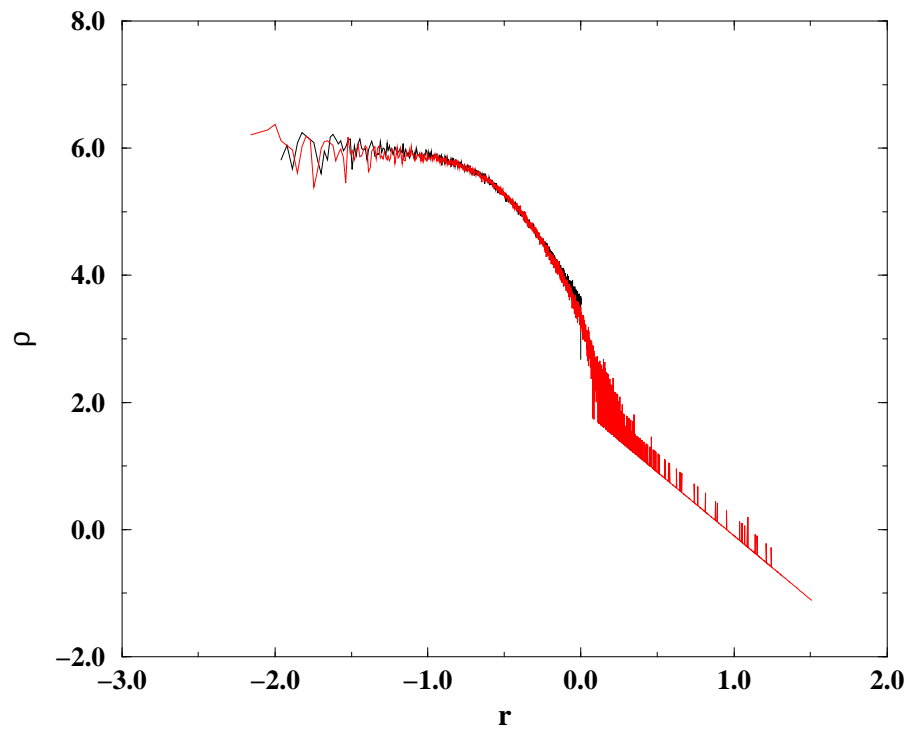


**FIG. 6.** Mass density of the system as a function of the distance from the center (in logarithmic scales and in model units), in the case of the system without the black hole, at  $t=0$  (black line) and at  $t=10 t_c$  (red line).

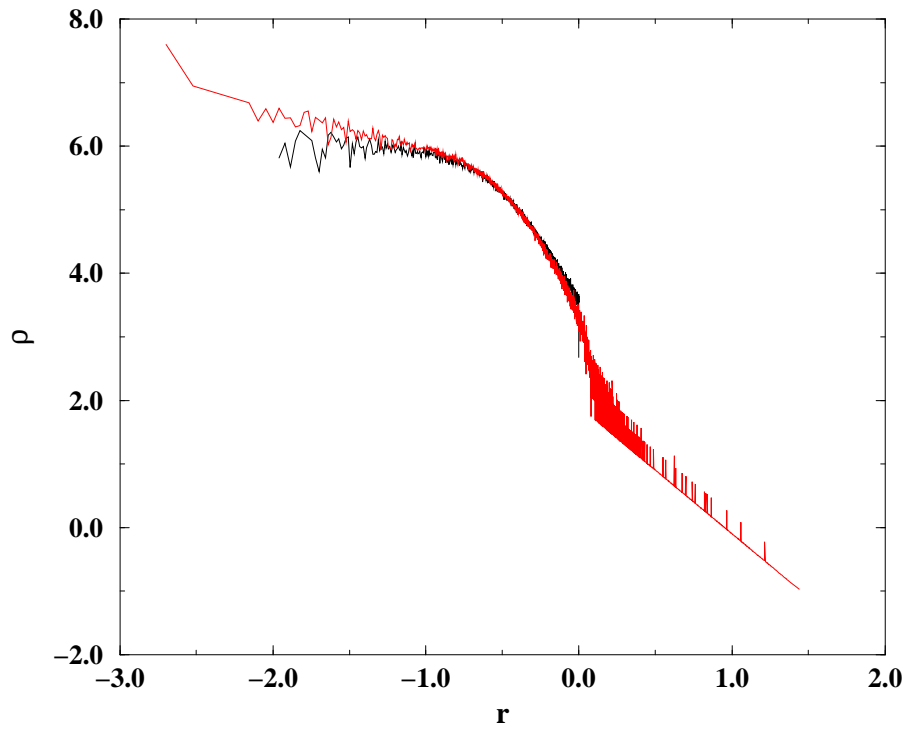


**FIG. 7.** Mass density of the system as a function of the distance from the center (in logarithmic scales and in model units) in the case  $m_{BH}=0.02$  at  $t=0$  (black line) and at  $t=10 t_c$  (red line).

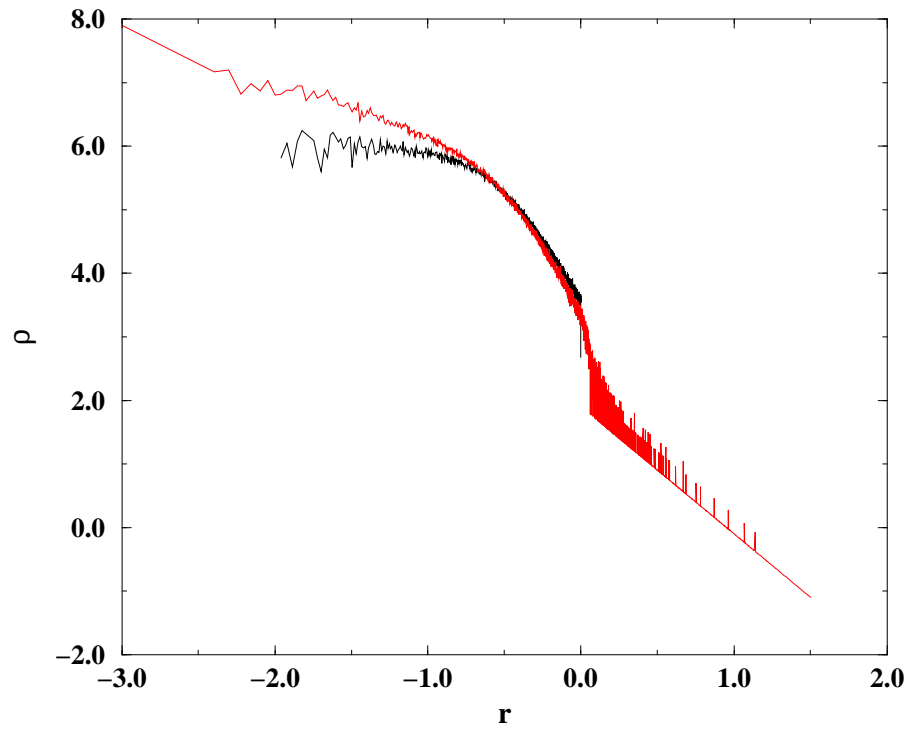


**FIG. 8.** Mass density of the system as a function of the distance from the center (in logarithmic scales and in model units) in the case  $m_{BH}=0.1$  at  $t=0$  (black line) and at  $t=10 t_c$  (red line).

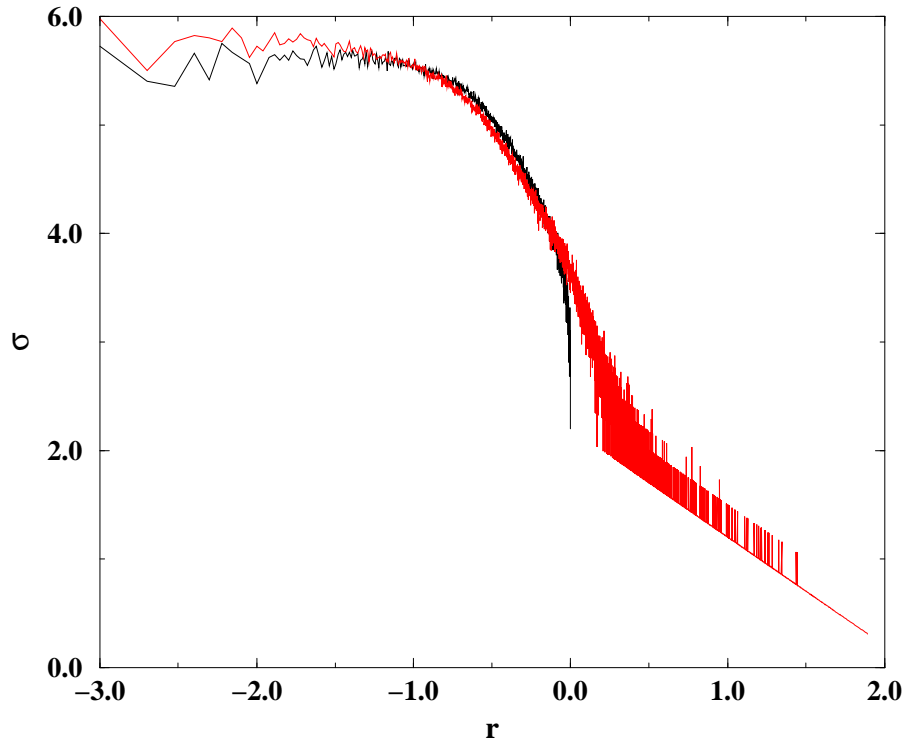


**FIG. 9.** Projected mass density of the system as a function of the distance from the black-hole (in the case  $m_{BH}=0.1$ ) at  $t=0$  (black line) and at  $t=10 t_c$  (red line).

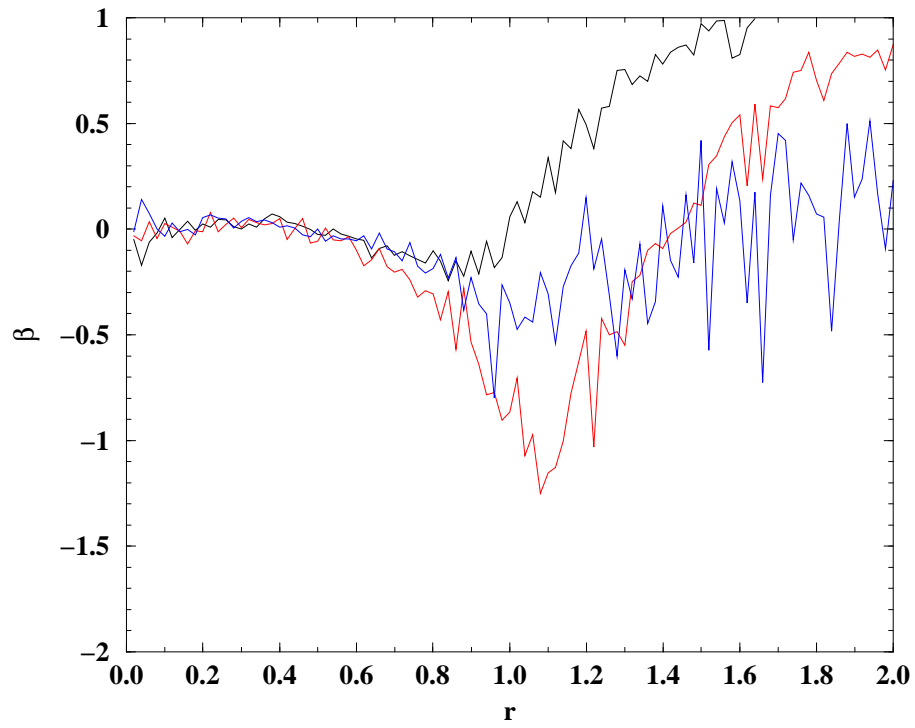


**FIG. 10.** Anisotropy parameter  $\beta$  (in model units) for the  $\theta$  component of the velocity for the system without the black hole at  $t=0.3 t_c$  (black line),  $t=1 t_c$  (red line),  $t=10 t_c$  (blue line).

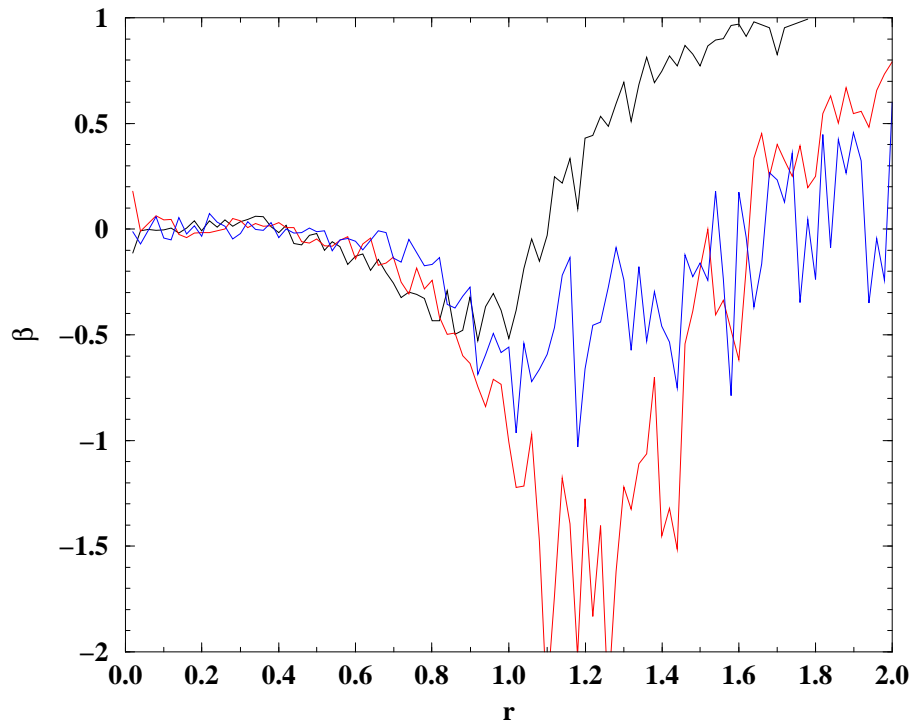


**FIG. 11.** Anisotropy parameter  $\beta$  (in model units) for the  $\theta$  component of the velocity for the system with  $m_{BH}=0.02$  at  $t=0.2 t_c$  (black line),  $t=1 t_c$  (red line),  $t=10 t_c$  (blue line).

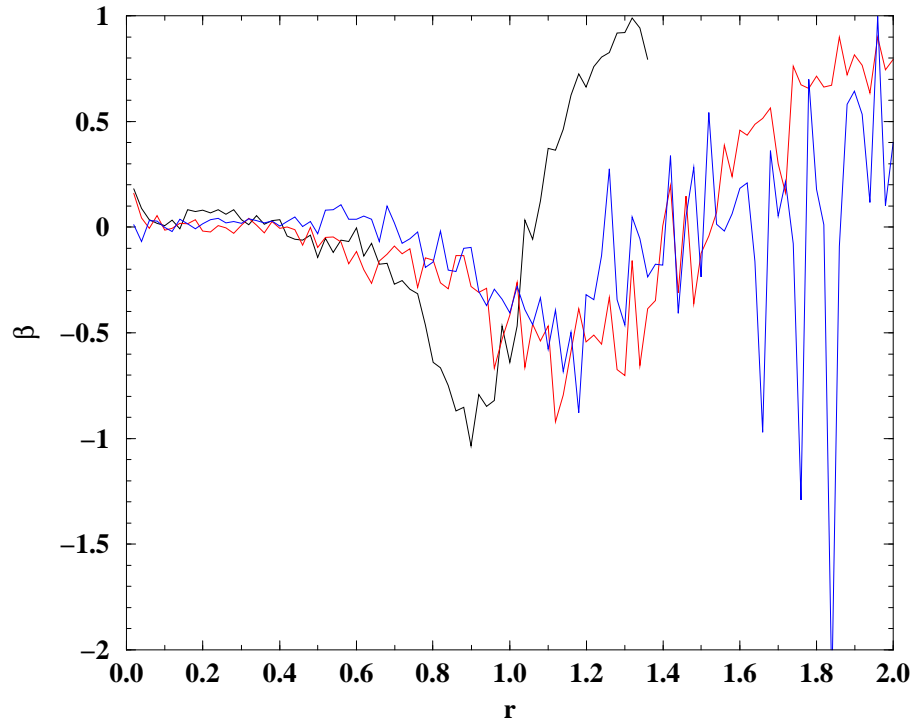


**FIG. 12.** Anisotropy parameter  $\beta$  (in model units) for the  $\theta$  component of the velocity for the system with  $m_{BH}=0.1$  at  $t=0.2 t_c$  (black line),  $t=1 t_c$  (red line),  $t=10 t_c$  (blue line).